Aerothermoelastic Considerations for a Control Surface on an Air-Breathing Hypersonic Vehicle

by
Benjamin R. Szpak[1]
The Ohio State University, Columbus, OH, 43210

Honors Thesis Advisor
Dr. Jack J. McNamara

[1] Undergraduate Research Assistant, Department of Aerospace Engineering, 2036 Neil Ave.

Abstract

Air-breathing hypersonic vehicles have risen to the forefront of the aerospace research community in reaction to the requirements of NASA and the US Air Force. NASA has interest in developing a next generation Reusable Launch Vehicle and the US Air Force is interested in an unmanned hypersonic vehicle. Recent research has focused on developing comprehensive models in order to successfully design a vehicle capable of operating in the severe hypersonic environment. Due to the layout of this class of vehicle, where the propulsion system is fully integrated into the lifting body fuselage, a tight coupling exists between the airframe, propulsion system, control system, and aerodynamics. This characteristic necessitates a multi-disciplinary approach to modeling for control design. To achieve this, a simplified model of each subsystem is needed to efficiently perform a multi-disciplinary analysis. Two important and challenging areas for multi-disciplinary modeling are the incorporation of complex aerodynamic and aerothermoelastic phenomena. The focus of this research is on the development of a model for the control surface. Specifically an aerothermoelastic model, based on a plate representation, has been developed for the vehicle control surface. This model was adapted from a previous model, developed at the Air Force Research Laboratory, to incorporate important characteristics such as taper and sweep of the control surface. Thus, the model more realistically represents the geometry of a control surface for a hypersonic vehicle. The structural model developed was then verified using finite element analysis to compare the free vibration frequencies and modeshapes. Since the structural dynamic characteristics of a solid plate are not compatible to those of a shell structured wing, the structural properties were modified to match the first two frequencies of a representative wing, namely the F-104 Lockheed Starfighter wing. As the temperature of a plate

increases, the first two frequencies begin to coalesce. This coalescence of frequencies leads to a phenomena known as flutter. As the temperature of the plate was increased the aerothermoelastic response was computed at a constant Mach number until the onset of flutter. By implementing a flexible control surface model, the response of the wing to control inputs and fuselage deformations could also be investigated. Both of these effects are modeled as base motion of the cantilevered plate. Second order piston theory, a commonly used model for hypersonic aerodynamics, was used to calculate the aerodynamic forces on the plate. Results presented provide insight into the importance of aerothermoelastic effects for control oriented modeling, as well as the effect of plate sweep and taper compared to a simple square plate representation.

Table of Contents

List of Figures vi

List of Tables vii

Nomenclature viii

Introduction and Objectives 1

A. Introduction 1

B. Literature Review 3

C. Objectives of this Thesis 6

D. Key Contributions from this Research 7

Derivation of Equations of Motion 8

A. Generalized Forces 9

B. Equations of Motion 11

C. Numerical Spatial Integration using Gaussian Quadrature 14

D. Determining Flutter Mach Number Using the P-Method 16

Model Validation and Studies 17

A. Validation of Control Surface Structural Model 17

B. Temperature Distribution 21

C. Modal Frequencies with Varying Geometries 22

D. Effect of Control Surface Geometry on Aerothermoelastic Response 24

E. Tip Displacement with Control Inputs 26

Conclusions 29

Matlab Functions 30

A. Pre_HSC_CS.m 30

B. thermal_mtx.m 31

C. ae_genforce.m 31

D. HSV_CS_ae.m 32

E. p_method.m 32

References 33

List of Figures

Figure 1. Two Dimensional Model of the X-43 2

Figure 2. Variation in the Flutter Mach Number of a Double Wedge Typical Section, as a Function of Elastic Axis Offset Parameter $\boldsymbol{a}$, Computed Using Different Orders of Piston Theory[9] 3

Figure 3. Variation in the Flutter Mach Number of a Double Wedge Typical Section, as a Function of Elastic Axis Offset Parameter $\boldsymbol{a}$, Computed Using Different Aerodynamic Models[9] 4

Figure 4. Degree of Coupling for the Domain of Aerothermoelasticity[9] 4

Figure 5. Piston Theory Visual Representation 10

Figure 6. F-104 Model Modeshapes 20

Figure 7. Square Flat Plate Modeshapes 20

Figure 8. Tapered, Swept Flat Plate Modeshapes 17

Figure 9. Normalized Temperature Distribution Used for Control Surface Heating 18

Figure 10. Natural Frequencies for a Thermally Stressed Square Plate, r = 1, θ = 0 23

Figure 11. Natural Frequencies for a Thermally Stressed Tapered/Swept Plate, r = 0.75, θ = 5 .. 24

Figure 12. Flutter Mach Number as Temperature Increases at Varying Taper Ratios 25

Figure 13. The Effect of Sweep on Flutter Mach Number 17

Figure 14. Inputs Used to Compute the Dynamic Response of the Control Surface Model 18

Figure 15. Tip Displacement Caused by Control Inputs 19

List of Tables

Table 1. Material Properties and Geometry for Control Surface Model..... 18

Table 2. Comparison of Control Surface Parameters to F-104 Wing..... 18

Table 3. Frequency Comparison Between the Matlab Model and Finite Element Solution..... 19

Nomenclature

$[\mathbf{A}]$ = stress function matrix

A = plate surface area

a = non-dimensional offset between elastic axis and the midchord of a double-wedge airfoil; positive for elastic axis behind midchord

a_∞ = freestream speed of sound

b = semi-chord

C_D, C_{Dp}, C_{Dv} = total coefficient of drag, pressure coefficient of drag, and viscous coefficient of drag, respectively

C_p,ΔC_p = coefficient of pressure and difference between coefficient of pressure between upper and lower surfaces, respectively

$[\mathbf{C^A}]$ = aerodynamic damping matrix

D = plate stiffness parameter, $\frac{Et_p^3}{12(1-\nu^2)}$

E = Young's Modulus

F = stress function

$\bar{F}$ = stress function amplitude

f = function that satisfies the stress function boundary condition on edges not geometrically constrained

g = function that satisfies the displacement geometric boundary conditions

h = rigid body plunge displacement

I_α = mass moment of inertia about the Elastic Axis

$\mathbf{J}$ = Jacobian

$[\mathbf{K}]$ = stiffness matrix

$[\mathbf{K^A}]$ = aerodynamic stiffness matrix

$[\mathbf{K^T}]$ = incremental stiffness matrix due to thermal stresses

$[\mathbf{M}]$ = mass matrix

M_∞ = freestream Mach number

m = mass per unit span

n_m = number of modes

$p(x,t)$ = aerodynamic surface pressure

p_∞ = freestream pressure

$\{\mathbf{Q}\}$, Q_i = generalized force vector, and generalized force of i^{th} mode, respectively

$\{\mathbf{Q^I}\}$,$\{\mathbf{Q^A}\}$ = generalized force vector due to inertial and aerodynamic forces, respectively

$\{\mathbf{q}\}$,q_i = vector of modal amplitudes, and i^{th} modal amplitude, respectively

q_∞ = freestream dynamic pressure

r = control surface taper ratio, $\frac{tip\ chord}{root\ chord}$

T = kinetic energy

$\Delta T(x,y,t)$ = change in temperature distribution in the plate
t = time
t_h = airfoil half thickness
t_p = plate thickness
U = elastic strain energy
V_∞ = freestream velocity
v_n = velocity of surface normal to the flow
w = vertical displacement of surface due to deformation
x, y = in-plane spatial variables
y_p = pivot location of the control surface
$Z(x,y,t)$ = vertical position of surface
$Z_{str}(x,y,t)$ = function describing the shape of the aerodynamic surface
α = rigid body pitch or angle of attack
α_{th} = coefficient of thermal expansion
β_s = oblique shock angle
γ = ratio of specific heats
η, ξ = local coordinates
θ = control surface sweep angle
ν = Poisson's ratio
ρ = plate density
ρ_∞ = freestream density
τ = airfoil thickness ratio; $\tau = \frac{t_h}{b}$
ϕ_i = vector of displacement for mode i
ω_α, ω_h = natural frequencies of uncoupled pitch and plunge motions
$\dot{(\,)}, \ddot{(\,)}$ = first and second derivatives with respect to time
$(\,)_x, (\,)_y, (\,)_z$ = differentiation with respect to x, y, or z, respectively

Introduction and Objectives

A. Introduction

NASA's interest in a Reusable Launch Vehicle (RLV) and the US Air Force's desire for unmanned hypersonic vehicles has invigorated hypersonic flight vehicle research. The need for next generation technology is emphasized by the space shuttles scheduled retirement in 2010 and the immediate plan for space access reverting to launch systems similar to those used during the Apollo era.

Currently, NASA is performing research to develop a Single-State-To-Orbit or Two-Stage-To-Orbit RLV capable of taking off and landing on a conventional runway. Also, the US Air Force's FALCON (Force Application and Launch from Continental US) program is focused on developing air-breathing hypersonic launch vehicles that will transport 12,000lbs of cargo up to 17,000km in less than 2 hours.[1] The goal of future hypersonic vehicles is to utilize air-breathing propulsion configurations since they do not require an onboard oxidizer for combustion, thus reducing overall vehicle weight. The NASA X-43 experimental vehicle has demonstrated air-breathing technology using a SCRamjet (Supersonic Combustion Ramjet) engine to set the world speed record for an air-breathing vehicle (Mach 9.6).

The boundary that separates hypersonic flight from supersonic flight is not set at a particular Mach number but it is best defined as that regime where nonlinear flow phenomena become progressively more important with increasing Mach number.[2] One example is increasing viscous interactions with Mach number caused by the rapid growth of the boundary layer and movement of the shock towards the body surface.[3-5] A second example is the presence of extreme aerodynamic heating due to significant flow compression and viscous dissipation.[3-5]

Aerodynamic heating of the flow surrounding a hypersonic vehicle leads to different thermodynamic and transport properties, high heat-transfer rates, variable ratio of specific heats, possible ionization, and non-adiabatic effects from radiation.

Aerodynamic heating is an essential concern for the hypersonic vehicle airframe, since it degrades structural material properties and induces thermal stresses. Lowered stiffness, due to material degradation and thermal stresses results in a reduction in natural frequencies of the structure. Also, a feature of thermal stresses is that they can lead to increased coupling between the vibration modes of the structure, as well as thermal buckling. Each of these issues can significantly affect the aeroelastic behavior and controllability of a hypersonic vehicle.

A complicating feature of air-breathing hypersonic vehicles is the use of an integrated air-frame propulsion configuration, as illustrated in Fig. 1. For this type of vehicle, the lower fuselage surface is part of a scramjet propulsion system. Such a configuration results in a tight-coupling between the aerodynamic, control, structural, and propulsion systems that cannot be neglected in analysis and design of this class of vehicle.[2,3] The bow shock from the front of the vehicle compresses the air into the scramjet inlet. If the vehicle trajectory is different than design, the shock will not compress the flow ideally into the inlet which results in reduced performance.

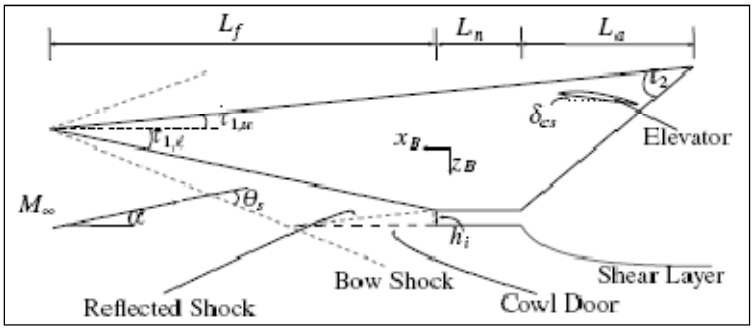

Figure 1. Two Dimensional Model of the X-43

An important aspect for a control-oriented model of hypersonic vehicles is simulation feasibility. In order to design a controller, the model must be executed over numerous repetitions for multiple potential vehicle trajectories. In order to meet this constraint, the refined model[6] was developed using a simple, experimentally validated, analytical flat plate model developed in Ref. [7]. The framework for the refined elevator model was completed by incorporating a commonly implemented, simple unsteady hypersonic aerodynamic theory known as "piston theory"[8].

B. Literature Review

Reference [9] describes comparisons that were made between first, second, and third order piston theory. The flutter Mach number was computed over a low aspect ratio wing. The low aspect ratio wing was considered representative of a HSV fin or control surface. It was shown that first order piston theory is unconservative when compared to both second and third order in computing the flutter Mach number over varying elastic axis offsets. Second and third order piston theory predict the flutter Mach number similarly for moderate to high Mach numbers, as shown in Fig. 2.

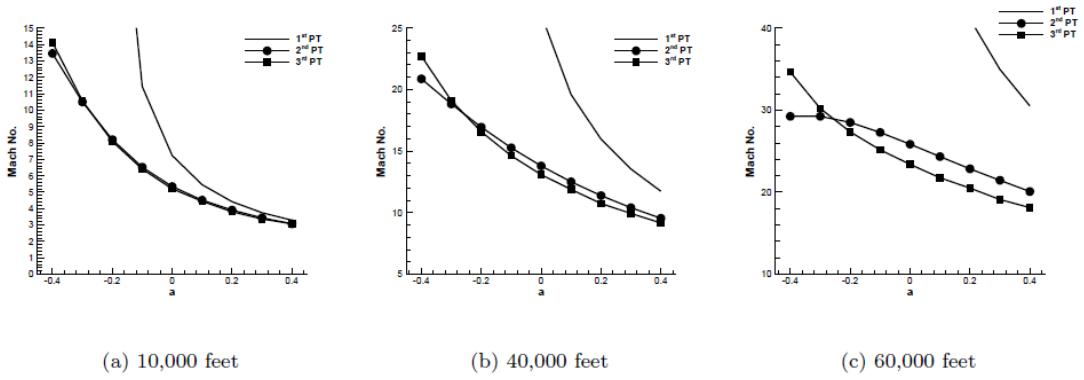

Figure 2. Variation in the Flutter Mach Number of a Double Wedge Typical Section, as a Function of Elastic Axis Offset Parameter a, Computed Using Different Orders of Piston Theory[9]

The accuracy of these predictions is shown by comparing third order piston theory to solutions computed using Navier-Stokes and Euler CFD solutions. Third order piton theory predicted similar results to the high fidelity solutions, varying by only 5-8%. This comparison is shown in Fig. 3. However, when the entire vehicle was considered, the error grew to over 25%. This is because the flow becomes highly three dimensional when the interaction between the lifting body and the control surface are considered.

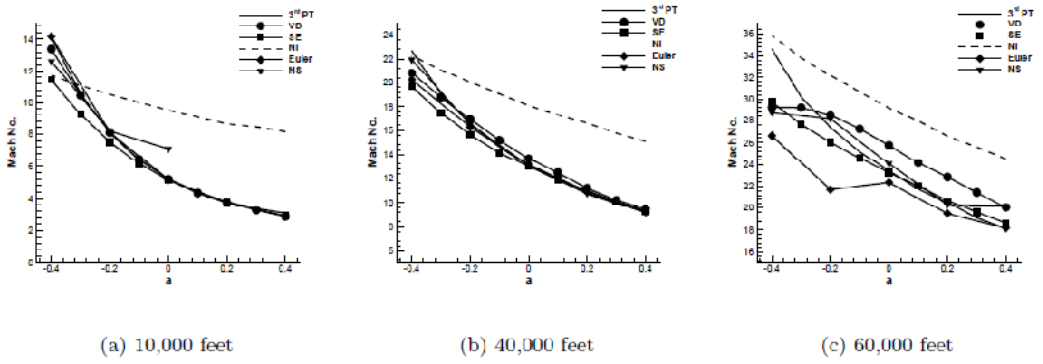

Figure 3. Variation in the Flutter Mach Number of a Double Wedge Typical Section, as a Function of Elastic Axis Offset Parameter a, Computed Using Different Aerodynamic Models[9]

Aerodynamic heating of control surfaces is described in Ref. [9]. When considering heating there are both strong and weak interactions as shown in Fig. 4.

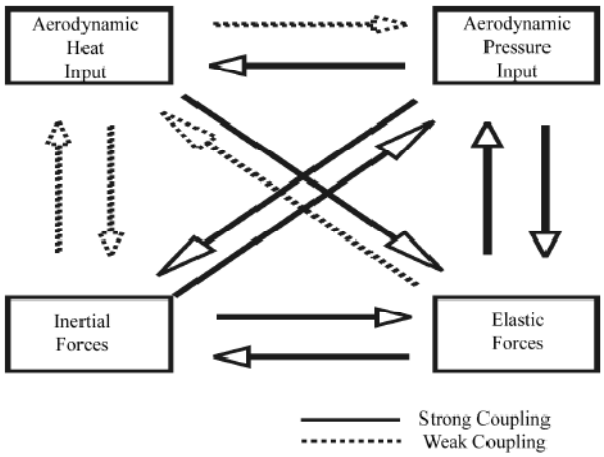

Figure 4. Degree of Coupling for the Domain of Aerothermoelasticity[9]

Aerothermoelastic problems can typically be simplified by neglecting the "weak" coupling shown in Fig. 4, as well as the effect of aerodynamic pressure on the aerodynamic heating. This reduces the problem to an aerothermal problem and a separate aeroelastic problem. This is based on three important assumptions:[9] 1) thermodynamic coupling between heat generation and elastic deformation is negligible; 2) dynamic aeroelastic coupling is small, i.e. the heating timescale is large when compared to the aeroelastic timescale; and 3) static aeroelastic coupling is small, i.e. elastic deflections are not large enough to alter the temperature distribution. There are few published studies of hypersonic aerothermoelasticity and because of the difficult nature of the problem; each study has varying degrees of accuracy.

A previous model for a HSV has been created at the Air Force Research Laboratory.[6] In this model, the elevator was assumed to be a rigid, two-dimensional flat surface. This is a questionable assumption since in reality the control surface will exhibit flexibility, which changes as a function of time due to flow velocity and extreme aerodynamic heating. Thus, the lift force the actual surface can generate will be different from that of a rigid one. In order to incorporate these effects, McNamara[6] initiated development of a control-oriented model for the elevator that couples a flexible structure to the unsteady aerodynamics. Furthermore, it incorporates the effects of aerodynamic heating by computing the change in structural stiffness of the elevator due to a prescribed temperature distribution. McNamara's results showed that the lift predictions between a rigid and a flexible control surface model varied by less than 3%.[6] This was primarily attributed to the fact that there was little change in angle of attack due to aeroelastic deformation.[6]

C. Objectives of this Thesis

From this introduction and literary review, it has been determined that improving the current models for HSV control surfaces is an important topic. The model created by McNamara[6] does not consider the typical geometry of a control surface. The primary objective of this thesis is to modify the model developed by McNamara[6] to incorporate the geometric properties of taper and sweep. This will allow for studies to be conducted concerning the effect of taper and sweep on key attributes such as the flutter margin at along a particular trajectory as well as the lift characteristics of the flexible control surface due to various control inputs.

The specific objectives of this thesis are:

1. To develop an aerothermoelastic model for a HSV control surface. This model will include structural flexibility, unsteady aerodynamics, and a prescribed heating distribution over the control surface. This model will include the geometric properties of taper and sweep of the control surface.
2. To compute the flutter margin for the control surface along a specified trajectory with varying geometries. This will determine the impact geometry has on aerothermoelastic characteristics of the control surface. Also, this will determine the performance characteristics of the control surface by determining the temperature at which the control surface will flutter.
3. Control inputs will be applied to the control surface throughout a specified trajectory to determine the effect of geometry on the displacement characteristics of the control surface.

Accomplishing these tasks will provide insight into the effect of taper and sweep on control surface aerothermoelastic properties and control surface effectiveness.

D. Key Contributions from this Research

1. The entire control based simulation takes approximately 15 minutes on a 2.4 GHz dual-core processor. This is important because the entire air-breathing HSV must be modeled at one time, so computational efficiency is essential. The model developed could be easily incorporated into a model of an entire HSV to provide the model with a representation of the control inputs.
2. Insight has been provided to the performance feasibility of a hypersonic control surface, and the effect geometry on performance. Once the flutter Mach number is lowered to the flight speed the control surface will flutter. This model considers only a contrived heating distribution, but still provides information on the flutter characteristics of a HSV control surface.

Derivation of Equations of Motion

Past research has indicated that the control surfaces on hypersonic vehicles are sensitive to aerothermoelastic phenomena and aerodynamic heating.[9] Aerodynamic heating leads to material property degradation of the structure, and also introduces thermal stresses. The latter effect leads to modal coupling of the structure[7] and thermal buckling.[9] These effects, in conjunction with the presence of aerodynamic pressures and excitation due to fuselage motion and control inputs, may have a significant impact on the response of control surfaces and the forces they are required to generate.

The previous model assumes that the control surfaces are composed of two dimensional, flat, rigid surfaces. This assumption was changed in Ref. [6] to incorporate structural flexibility and aerodynamic heating. State-of-the-art aerothermoelastic modeling approaches utilize finite element models of the structure, in conjunction with CFD-based unsteady aerodynamic loads.[9] However, due to computational constraints, such an approach is impractical for the control-oriented hypersonic vehicle model. As an alternative, a model was developed based on an equivalent plate structure and second order piston theory aerodynamics. A historical basis for such a model is presented in Ref. [6]. The procedure for deriving the governing equations described herein is derived from Ref. [6].

In Ref. [7], a theoretical approach is provided for finding the free-vibration characteristics of thermally stressed plates subject to various boundary conditions. For the control surface model, a cantilevered plate represents the appropriate boundary conditions. In Bailey's[7] formulation, Reissner's energy functional for a plate is solved using a Rayleigh-Ritz procedure, where the spatial dependence of the plate unknowns is represented using simple polynomial expressions. For the current model, Bailey's formulation was modified by including the effects of rigid body

plunge and pitch of the airfoil (related to the motion of the fuselage and control inputs) and also aerodynamic forces due to the hypersonic flow. The equations for the control surface were then re-derived using Lagrange's equations:

$$\frac{d}{dt}\left(\frac{\delta T}{\delta \dot{q}_i}\right) - \frac{\delta T}{\delta q_i} + \frac{\delta U}{\delta q_i} = Q_i \quad i = 1,2,\dots,n_m \tag{1}$$

The total kinetic energy in the system will consist of components due to surface flexibility, as well as rigid body pitch and plunge motions, i.e.:

$$T = \int\int \left\{\frac{1}{2}\rho t_p\left(\dot{w} - \dot{h} - (y - y_p)\dot{\alpha}\right)^2\right\} dA \tag{2}$$

In the kinetic energy equation $\dot{w}$ is the velocity of any point on the control surface due to the flexible structure. There is also kinetic energy associated with rigid body pitch and plunge of the control surface, $\dot{h}$ and $\dot{\alpha}$ respectively. Rigid body pitch is caused by the control inputs to the control surface in order to change the attitude of the vehicle. The rigid body plunge is related to the motion of the fuselage which moves the control surface at the root.

The strain energy for a thermally stressed, thin, homogeneous plate with no initial deflection is given by Bailey as:[7]

$$\begin{aligned} U = \int\int \Big\{ & \frac{D}{2}\left[w_{xx}^2 + w_{yy}^2 + 2\nu w_{xx}w_{yy} + 2(1-\nu)w_{xy}^2\right] \\ & + \frac{t_p}{2}\left[F_{xx}w_y^2 + F_{yy}w_x^2 - 2F_{xy}w_x w_y\right] \\ & - \frac{t_p}{2E}\left[F_{xx}^2 + F_{yy}^2 - 2\nu F_{xx}F_{yy} + 2(1+\nu)F_{xy}^2\right] \\ & - t_p\alpha_{th}\Delta T(x,y,t)\left[F_{xx} + F_{yy}\right]\Big\} dA \end{aligned} \tag{3}$$

A. Generalized Forces

The generalized force of the surface of the control surface due the aerodynamic pressures is give by:

$$Q_i^A = q_\infty \int \int \phi_i \Delta C_p(\boldsymbol{q}, \dot{\boldsymbol{q}}, \ddot{\boldsymbol{q}}) dA \tag{4}$$

The aerodynamic theory used for this model is Piston theory, see Fig. 5.

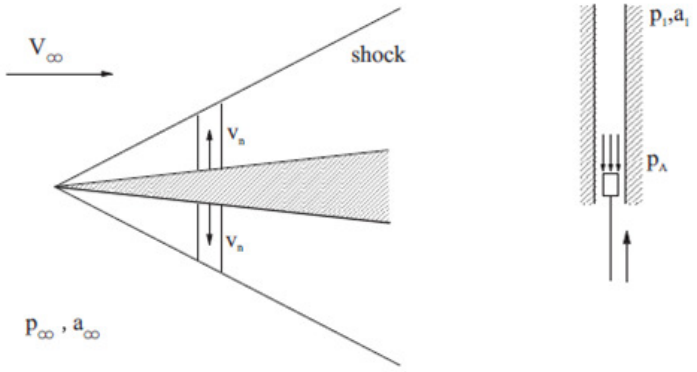

Figure 5. Piston Theory Visual Representation

Piston theory was developed by Lighthill[11]. Lighthill noticed that at high Mach numbers shock waves and expansion fans on an airfoil form at small angles to the undisturbed flow. This implies that streamwise gradients are small compared to gradients perpendicular to the flow. Since velocity components parallel to shock waves and expansion fans are unchanged, velocity components perpendicular to the flow are large compared to disturbances to components parallel to the flow. Consequently, any plane slab of fluid, initially perpendicular to the undisturbed flow, remains so as it is swept downstream and moves in its own plane. A simple expression for the unsteady aerodynamic pressure coefficient is provided by second order piston theory. This order of piston theory is selected since it captures important flow nonlinearities, while maintaining a linear relation with system state variables for airfoil shapes symmetric about the chordline.[8] Thus, the coefficient of pressure is defined as:

$$C_p(y,t) = \frac{2}{M_\infty^2}\left\{\frac{v_n}{a_\infty} + \frac{(\gamma+1)}{4}\left(\frac{v_n}{a_\infty}\right)^2\right\} \tag{5}$$

where

$$v_n = \frac{\partial Z(x,y,t)}{\partial t} + V_\infty \frac{\partial Z(x,y,t)}{\partial y} \tag{6}$$

The position of the control surface is a function of both flexible deformation, as well as rigid body motion associated with fuselage motion and control surface modulation. Thus, the position of the airfoil is given by:

$$Z(x,y,t) = w(x,y,t) - h(t) - \big(y - y_p\big)\alpha(t) + Z_{str}(x,y) \tag{7}$$

Where w is the position of the control surface due to structural flexibility, h and α are the position due to rigid body pitch and plunge, and Z_{str} is the aerodynamic shape of the control surface, assumed to be a symmetric double wedge.

B. Equations of Motion

There are two unknowns in the equations of motion, namely structural deformation $w(x,y,t)$ and the in-plane stress function $F(x,y,t)$ due to the presence of thermal stresses. Following the formulation of Bailey,[7] let:

$$\begin{aligned} w(x,y,t) &= g(x,y)\sum_i \sum_j q_{ij}(t)x^i y^j \\ F(x,y,t) &= f(x,y)\sum_r \sum_s \bar{F}_{rs}(t)x^r y^s \end{aligned} \tag{8}$$

Also, Bailey[7] notes that for small displacements the stress function $F(x,y,t)$ can be solved independently of $w(x,y,t)$. Thus, the stress function relation provided in Ref. [7] is also used here to determine the coefficients of the stress function:

$$\{\bar{F}(t)\} = -\alpha_{th}[A]^{-1}\{\Gamma\} \tag{9}$$

where

$$A_{pqrs} = \int\int \frac{1}{E}\{(fx^p y^q)_{xx}(fx^r y^s)_{xx} + (fx^p y^q)_{yy}(fx^r y^s)_{yy} - \nu\left[(fx^p y^q)_{xx}(fx^r y^s)_{yy} + (fx^p y^q)_{yy}(fx^r y^s)_{xx}\right] + 2(1+\nu)(fx^p y^q)_{xy}(fx^r y^s)_{xy}\}dA \tag{10}$$

and

$$\Gamma_{rs} = \int\int \Delta T(x,y,t)\left[(fx^r y^s)_{xx} + (fx^r y^s)_{yy}\right] dA \tag{11}$$

Using Eqn. (1) to (11), the equations of motion for the plate are given by:

$$[\mathbf{M}]\{\ddot{\mathbf{q}}\} + [\mathbf{C^A}]\{\dot{\mathbf{q}}\} + \left([\mathbf{K}] + [\mathbf{K^T}] + [\mathbf{K^A}]\right)\{\mathbf{q}\} = \{\mathbf{Q}\} \tag{12}$$

where

$$M_{ijkl} = \int\int \left\{\frac{1}{2}\rho t_p g(x,y)^2 x^{i+k} y^{j+l}\right\} dA \tag{13}$$

$$C^A_{ijkl} = \int\int \left\{\frac{1}{2} a_\infty M_\infty g(x,y)^2 x^{i+k} y^{j+l}\left(4 - M_\infty(\gamma+1)\left(\left.\frac{\partial Z_{str}}{\partial y}\right|_l - \left.\frac{\partial Z_{str}}{\partial y}\right|_u\right)\right)\right\} dA \tag{14}$$

$$K_{ijkl} = \int\int \frac{D}{2}\left\{\left(gx^i y^j\right)_{xx}\left(gx^k y^l\right)_{xx} + \left(gx^i y^j\right)_{yy}\left(gx^k y^l\right)_{yy} + \nu\left[\left(gx^i y^j\right)_{xx}\left(gx^k y^l\right)_{yy} + \left(gx^i y^j\right)_{yy}\left(gx^k y^l\right)_{xx}\right] + 2(1+\nu)\left(gx^i y^j\right)_{xy}\left(gx^k y^l\right)_{xy}\right\} \tag{15}$$

$$K_{ijkl}^{T} = \sum_{p}\sum_{q} \bar{F}_{pq} \int\int \Big\{ (fx^p y^q)_{yy} \left(gx^i y^j\right)_x \left(gx^k y^l\right)_x + (fx^p y^q)_{xx} \left(gx^i y^j\right)_y \left(gx^k y^l\right)_y - (fx^p y^q)_{xy} \Big[\left(gx^i y^j\right)_x \left(gx^k y^l\right)_y + \left(gx^i y^j\right)_y \left(gx^k y^l\right)_x \Big] \Big\} dA \tag{16}$$

$$K_{ijkl}^{A} = \int\int \left\{ \frac{1}{2} a_\infty^2 M_\infty \rho_\infty g(x,y) x^i y^j \left(4 - M_\infty(\gamma+1) \left(\left.\frac{\partial Z_{str}}{\partial y}\right|_l - \left.\frac{\partial Z_{str}}{\partial y}\right|_u \right) \right) \right\} dA \tag{17}$$

and:

$$\{\mathbf{Q}\} = \{\mathbf{Q^I}\} + \{\mathbf{Q^A}\} \tag{18}$$

$$Q_{ij}^{I} = \int\int \{\rho t_p \ddot{h} g(x,y) x^i y^j\} dA + \int\int \{\rho t_p (y - y_p) \ddot{\alpha} g(x,y) x^i y^j\} dA \tag{19}$$

$$Q_{ij}^{A} = \int\int \left\{ \left(\frac{1}{2}\dot{h}a_{\infty}M_{\infty}g(x,y)x^{i}y^{j} \right.\right.$$
$$- \frac{1}{4}a_{\infty}^{2}M_{\infty}\rho_{\infty}g(x,y)x^{i}y^{j}\left(\left.\frac{\partial Z_{str}}{\partial y}\right|_{l} + \left.\frac{\partial Z_{str}}{\partial y}\right|_{u} \right)$$
$$+ \frac{1}{2}\alpha a_{\infty}^{2}M_{\infty}\rho_{\infty}g(x,y)x^{i}y^{j} \qquad (20)$$
$$\left. + \frac{1}{2}\dot{\alpha}a_{\infty}\rho_{\infty}g(x,y)x^{i}y^{j}(y-y_{p}) \right)\left(4 \right.$$
$$\left.\left. - M_{\infty}(\gamma+1)\left(\left.\frac{\partial Z_{str}}{\partial y}\right|_{l} - \left.\frac{\partial Z_{str}}{\partial y}\right|_{u} \right) \right) \right\} dA$$

The stiffness term includes structural stiffness, thermal stiffness, and aerodynamic stiffness matrices. The thermal stiffness matrix includes thermal stresses and lowers the structural integrity of the control surface. The forcing term includes inertial forces, due to the flexible structure, and aerodynamic forcing terms calculated using piston theory.

C. Numerical Spatial Integration using Gaussian Quadrature

Despite the use of polynomial functions, several of the above integrations are difficult to carry out analytically. Thus, second order Gaussian quadrature has been used to perform the spatial integrations.

Consider the following general integral statement:[10]

$$I = \int_{-1}^{1} h(\xi)d\xi \qquad (21)$$

Let the integral be approximated by the following n-point approximation:

$$I = \int_{-1}^{1} h(\xi) d\xi \approx w_1 h(\xi_1) + w_2 h(\xi_2) + \cdots + w_n h(\xi_n) \tag{22}$$

where $w_1, w_2, \ldots, w_n$ are weights and $\xi_1, \xi_2, \ldots, \xi_n$ are the sampling points, or Gauss points. The goal is to select the weights and sampling points such that the approximation provides an exact solution for polynomials $h(\xi)$ for as large a degree as possible.

For second order Gaussian quadrature (i.e. $n = 2$), this method is exact for a cubic polynomial. The weights and sampling points for second order Gaussian quadrature are:

$$\begin{aligned} w_1 &= 1.0 \\ w_2 &= 1.0 \end{aligned} \tag{23}$$

and

$$\begin{aligned} \xi_1 &= -\frac{1}{\sqrt{3}} \\ \xi_2 &= \frac{1}{\sqrt{3}} \end{aligned} \tag{24}$$

Thus, the integration is carried out by sampling the integrand at the points listed in Eqs. (24), and summing according to Eqn. (22).

In order to extend to a two-dimensional integral, the procedure becomes:

$$I \approx \sum_{i=1}^{n} \sum_{j=1}^{n} w_i w_j h(\xi_i, \eta_j) \tag{25}$$

Note that in general the discretized plate will not have square unit area elements. However, it can be shown that the integral in Eqn. (25) can be carried out using a transformation between a "local" $\xi - \eta$ coordinate frame and the global $x - y$ coordinate frame:[10]

$$dx\, dy = det\mathbf{J}\, d\xi\, d\eta \tag{26}$$

where **J** is the Jacobian of the transformation.

D. Determining Flutter Mach Number Using the P-Method

Using the equations of motion defined in Eqn. (12), the following definitions are made:

$$\{\dot{\mathbf{q}}\} = \{\mathbf{y_1}\}, \{\mathbf{q}\} = \{\boldsymbol{y_2}\} \tag{27}$$

Doing this redefines the generalized coordinates and allows for simplification of the equations. Then, the forcing terms are neglected to reduce the equations of motion to a homogeneous set of equations. This assumption removes the physical meaning in the transient response in the equations but the flutter boundary can still be accurately predicted.

$$[\mathbf{M}]\{\dot{\mathbf{y}}_\mathbf{1}\} + [\mathbf{C^A}]\{\mathbf{y_1}\} + \big([\mathbf{K}] + [\mathbf{K^T}] + [\mathbf{K^A}]\big)\{\mathbf{y_2}\} = \mathbf{0} \tag{28}$$

Defining the state vector as $\{\dot{\mathbf{y}}\} = \begin{Bmatrix} \dot{\mathbf{y}}_\mathbf{1} \\ \dot{\mathbf{y}}_\mathbf{2} \end{Bmatrix}$ the problem can be reduced to the simple eigenvalue problem:

$$\{\dot{\mathbf{y}}\} = \begin{Bmatrix} \dot{\mathbf{y}}_\mathbf{1} \\ \dot{\mathbf{y}}_\mathbf{2} \end{Bmatrix} = \begin{bmatrix} -[\mathbf{M}]^{-1}[\mathbf{C^A}] & -[\mathbf{M}]^{-1}\big([\mathbf{K}] + [\mathbf{K^T}] + [\mathbf{K^A}]\big) \\ [\mathbf{I}] & [\mathbf{0}] \end{bmatrix} \{\boldsymbol{y}\}$$
$$\text{or} \quad \{\dot{\mathbf{y}}\} = [\mathbf{A}]\{\boldsymbol{y}\} \tag{29}$$

The eivenvalues of $[\mathbf{A}]$ govern the solution of $\{\mathbf{y}\}$. The eigenvalues of $[\mathbf{A}]$ will yield two complex-conjugate pairs. The Mach number is incrementally increased and once the real part of one of these pairs becomes positive the flutter boundary has been reached.

Model Validation and Studies

The equations of motion for the control surface, listed in Eqs. (9) to (20), were coded into a series of Matlab functions. This section describes steps to validate these functions by comparing them to a finite element model. Then the effect of taper and sweep on aerothermoelastic response was evaluated.

A. Validation of Control Surface Structural Model

For the current control surface model, 25 polynomial terms were used to represent the spatial variation of the displacement and stress functions, i.e.:

$$w(x,y,t) = g(x,y)\sum_{i=0}^{4}\sum_{j=0}^{4} q_{ij}(t)x^i y^j$$

$$F(x,y,t) = f(x,y)\sum_{r=0}^{4}\sum_{s=0}^{4} \bar{F}_{rs}(t)x^r y^s \tag{30}$$

where the following functions were used to prescribe the geometric and stress boundary condition for a cantilever plate:

$$g(x,y) = \left(\frac{x}{a}\right)^2 \tag{31}$$

$$f(x,y) = \left(\frac{x}{a}-1\right)^3\left(\left(\frac{y}{b}+\frac{1}{2}\right)\left(\frac{y}{b}-\frac{1}{2}\right)\right)^3 \tag{32}$$

Equation (31) enforces zero displacement at the built-in section of the plate, while Eqn. (32) enforces a stress free boundary on the free edges of the plate.

The properties used for the plate are shown in Table 1.

Table 1. Material Properties and Geometry for Control Surface Model

E	79.1×10^9	Pa
ρ	550	kg/m^3
α_{th}	12.8×10^{-6}	per deg F
ν	0.333	
l_s	3.15	m
l_c	3.15	m
t_p	0.07	m
τ	0.0336	

These plate properties were chosen to match the important parameters for the F-104 Starfighter wing. The most important parameters when comparing aeroelastic effects are the mass, first bending frequency, first torsional frequency, and aspect ratio. Table 2 shows a comparison of the control surface to the F-104 wing parameters.

Table 2. Comparison of Control Surface Parameters to F-104 Wing

Parameter	**F-104**	**Control Surface**
Mass, kg	350	382
1st Bending Freq, Hz	13.40	14.28
1st Torsional Freq, Hz	37.60	34.60
Span, m	2.31	3.15
Max Chord, m	4.00	3.15
Lifting Area, m^2	6.7	9.2
AR	0.8	1.0

Finite element analysis was used to validate the structural model. After the taper and sweep characteristics incorporated into the model, the natural frequencies were extracted and compared to a finite element solution. For the finite element solution a 100 x 100 node grid, using CQUAD4 shell elements was used. The modes and frequencies of the structure were computed using the MSC.NASTRAN Normal Modes solution.

First, a square plate was considered. Then, the taper ratio was set to 0.5 with a sweep of 10 degrees. A taper ratio and sweep angle beyond the considered cases was used in order to ensure that the structural model is accurate for the entire range of cases. The frequencies from the model were compared with the finite element frequencies. Table 3 shows that the maximum error from the finite element solution and the approximate solution is less than 5%.

Table 3. Frequency Comparison between the Model and Finite Element Solution

	Square Plate, $r = 1, \theta = 0$			Tapered/Swept Plate, $r = 0.5, \theta = 10$		
	Frequency, Hz			Frequency, Hz		
Mode	Model	NASTRAN	%error	Model	NASTRAN	%error
1	14.28	14.23	0.37%	16.80	16.57	1.39%
2	34.62	34.21	1.18%	56.46	57.00	0.96%
3	87.10	86.48	0.72%	92.11	91.45	0.72%
4	112.63	110.60	1.84%	161.39	157.70	2.34%
5	127.01	124.60	1.94%	227.15	238.20	4.64%

The most important modes for aeroelastic analysis are the first bending and the first torsional modes. The model and NASTRAN models agree within 1.5% for these two modes, thus validating the structural model.

Modeshapes are another important consideration for aeroelastic studies. The modeshapes for a finite element model of the F-104 wing are shown in Fig. 6.

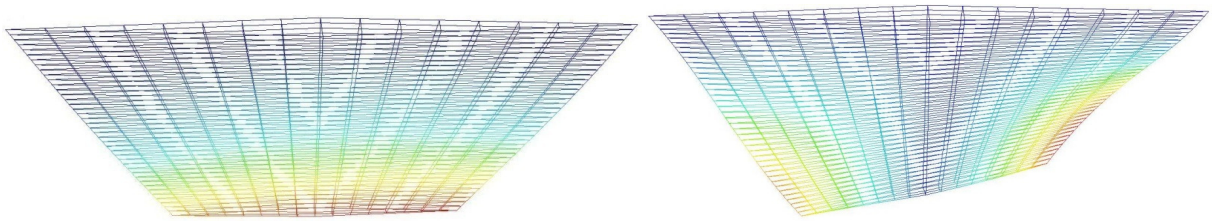

First Bending Mode First Torsion Mode

Figure 6. F-104 Model Modeshapes

The modeshapes for the tapered, swept structure are nonsymmetrical about the centerline. However when using a square plate representation of the control surface the modeshapes are completely symmetric about the centerline. This trend can be seen in Fig. 7.

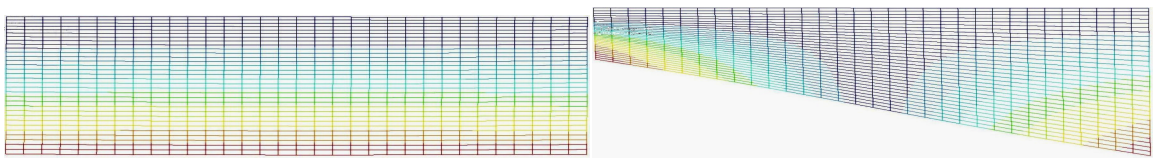

First Bending Mode First Torsion Mode

Figure 7. Square Flat Plate Modeshapes

The general trend of the modeshapes is still visible, however the asymmetric and symmetric features are cause for concern. The modeshapes are used to determine the displacement in the

control surface by the model. If the modeshapes are not representative of the actual structure then the displacement results are not going to match accurately. If taper and sweep are added into the flat plate model the modeshapes should match the F-104 wing structure more accurately. Figure 8 shows the effect of taper and sweep on the modeshapes.

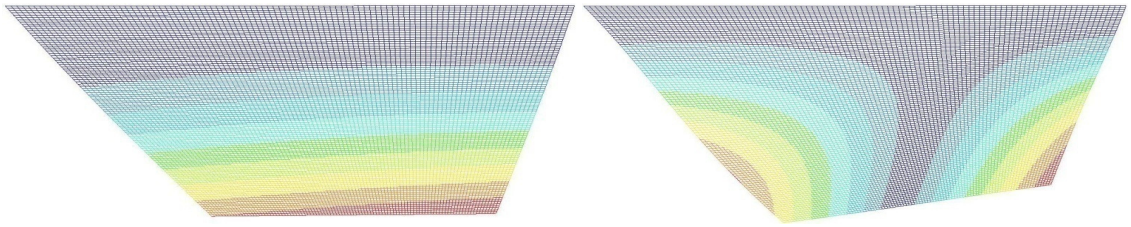

First Bending Mode First Torsion Mode

Figure 8. Tapered, Swept Flat Plate Modeshapes

The modeshapes for the tapered, swept plate represent the F-104's wing shell structure much more accurately. This indicates that a tapered, swept plate will displace in a similar manner to F-104 wing.

B. Temperature Distribution

The plate studied in Refs. [7] and [8] was a cantilever structure constructed from aluminum; with an aspect ratio of 1, a side length of 17.75 in., and a thickness of 0.1875 in. The plate was heated along the edges perpendicular to the built-in edge. For the experimental analysis, the temperature distribution was approximated from the measured experimental temperature distribution and scaled by a reference temperature, T_{ref}. Since the exact temperature distribution was not available for use in Ref. [8], an approximate distribution based on the description provided in Ref. [7] was used. This temperature distribution is used to heat the control surface model and is depicted in Fig. 9.

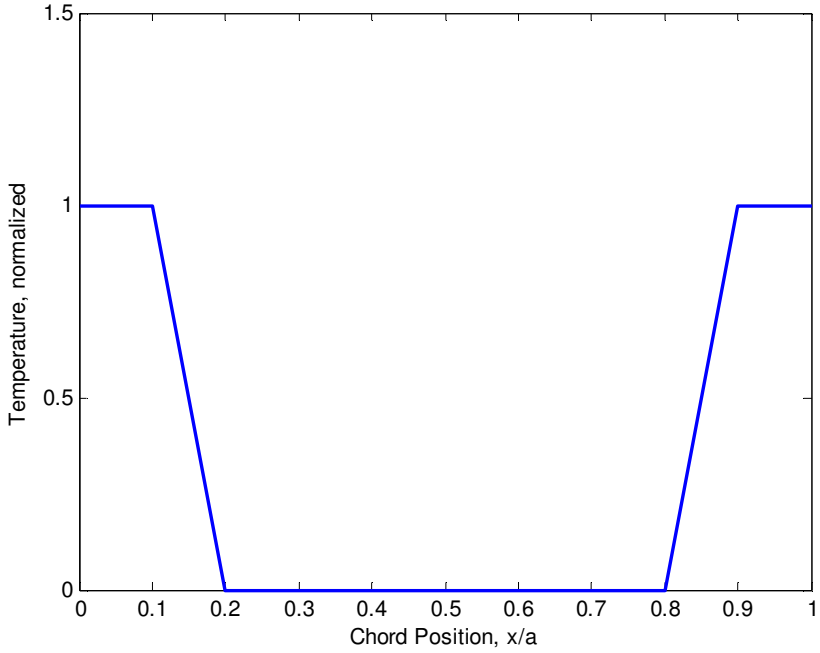

Figure 9. Normalized Temperature Distribution Used for Control Surface Heating

This temperature distribution is normalized and indicates heating at both the leading edge and trailing edge of the control surface. It is important to note that the temperature distribution used in this model is not representative of aerodynamic heating. The thermal model Bailey[7] used was confirmed from empirical results and was used in order to have verifiable results for the structural model. Also, there are significant differences between the heating of a shell structure and the heating of a solid, flat plate. These considerations are outside of the scope of this research and could be the focus of further research.

C. Modal Frequencies with Varying Geometries

The root cause of flutter is the frequency coalescence of the first bending and the first torsional modes. When including thermal stresses in the aeroelastic analysis, the heating lowers the modal frequencies. This effect can be seen in Fig. 10 below. No aerodynamic forces are being considered here, these are the plate's natural frequencies.

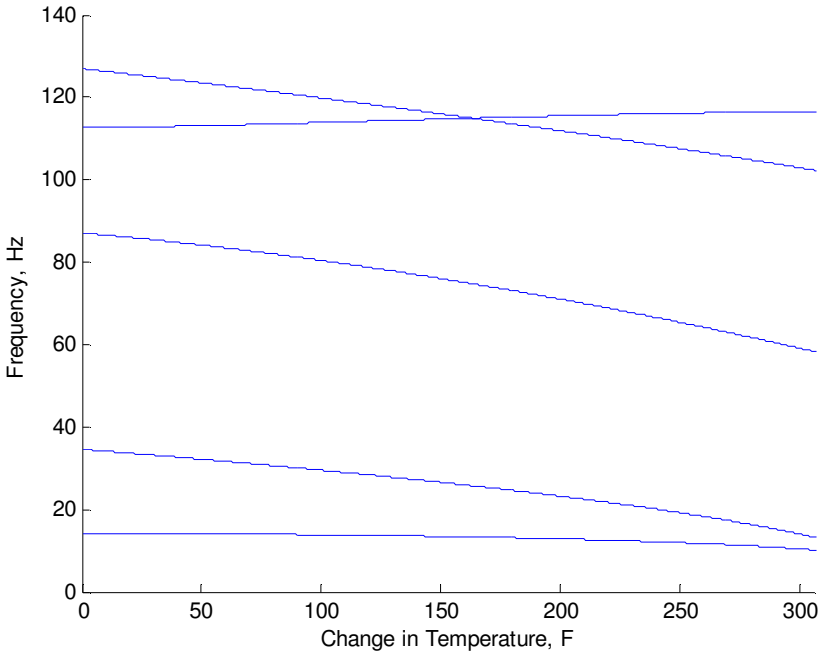

Figure 10. Natural Frequencies for a Thermally Stressed Square Plate, r = 1, θ = 0

The lowest two frequencies are the first bending and the first torsional modes. At the highest temperature the two modes are approaching each other. As the control surface is introduced to aerodynamic forces, the first two modes will couple together and begin to coalesce. This indicates that flutter will occur at lower Mach numbers as the temperature increases.

Alternately, if a tapered swept plate is considered the modal frequencies behave differently. Figure 11 shows the natural frequencies for a control surface with a taper ratio of 0.75 and a sweep of 5°.

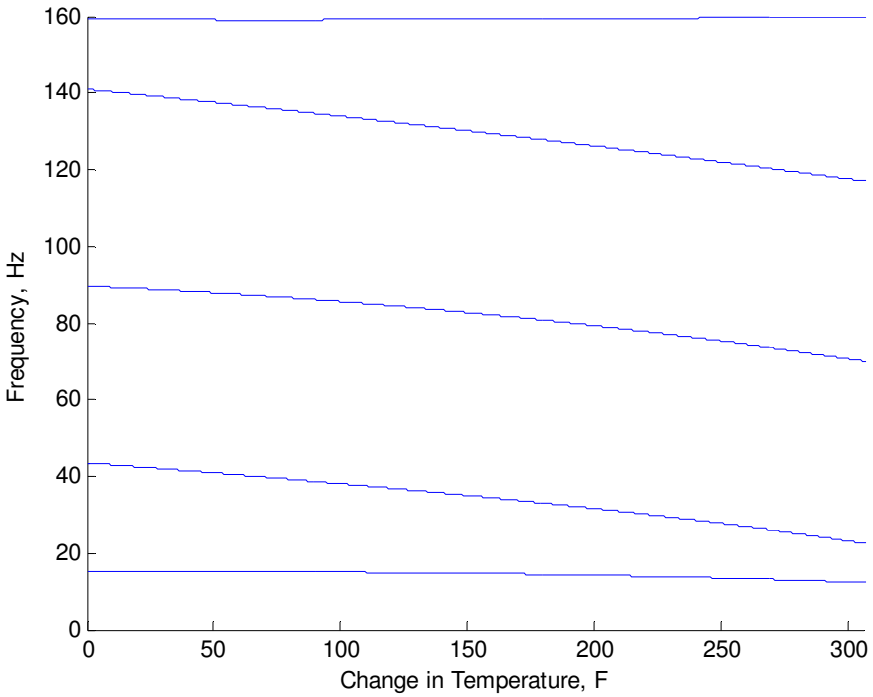

Figure 11. Natural Frequencies for a Thermally Stressed Tapered/Swept Plate, r = 0.75, θ = 5

Figure 11 shows that the effect of heating is less for a tapered, swept plate, i.e. there is a greater disparity between the first two modes at the maximum temperature. This implies that a tapered, swept control surface should have more desirable aerothermoelastic properties when compared to a square control surface.

D. Effect of Control Surface Geometry on Aerothermoelastic Response

As the taper ratio of the plate is decreased from 1 to 0.75, the flutter Mach number is increased uniformly across all temperatures. This trend is shown in Fig. 12.

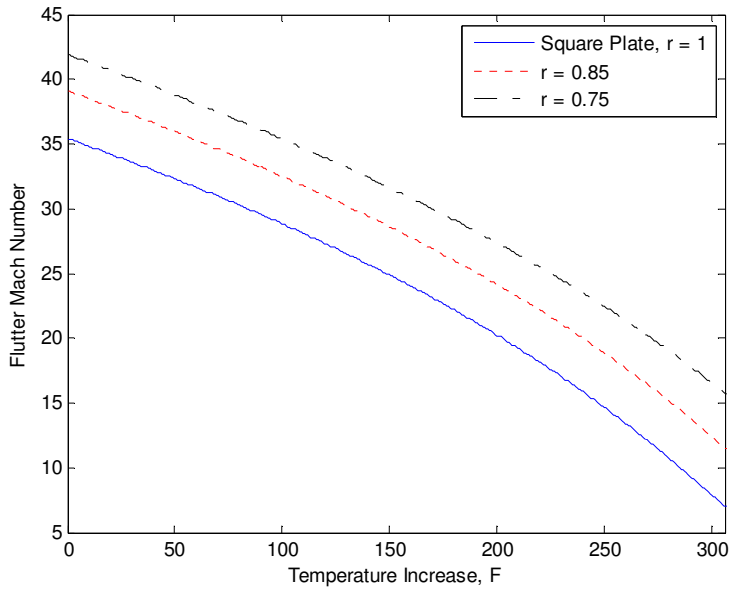

Figure 12. Flutter Mach Number as Temperature Increases at Varying Taper Ratios

This indicates that the heating of the control surface is still introducing thermal stresses at an equal rate in the tapered plate as it was for a square plate. However, adding taper to the control surface reduces the lifting area which reduces the aerodynamic coupling effects.

The sweep of the control surface actually reduces the effect that temperature has on the flutter Mach number. As the sweep of the wing is increased, the flutter Mach number at maximum temperature is increased. This trend is shown in Fig. 13.

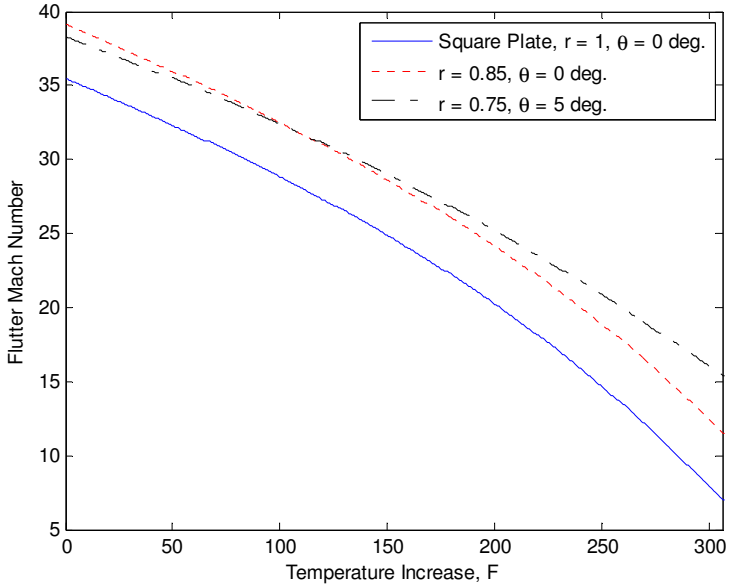

Figure 13. The Effect of Sweep on Flutter Mach Number

At low temperatures the flutter Mach number is decreased slightly when sweep is added. However, as the temperature increases there is a point, near a temperature increase of 100°F, where the flutter Mach number becomes larger for the swept plate.

E. Tip Displacement with Control Inputs

In order to exhibit the capabilities of the model developed, a dynamic study of the control surface response to different control inputs was implemented. The response of the plate to rigid body motions, aerodynamic pressures, and increasing temperature was computed. The operating conditions were held constant at Mach 12 at 85,000 feet. The rigid body motion of the plate was prescribed as shown in Fig. 14.

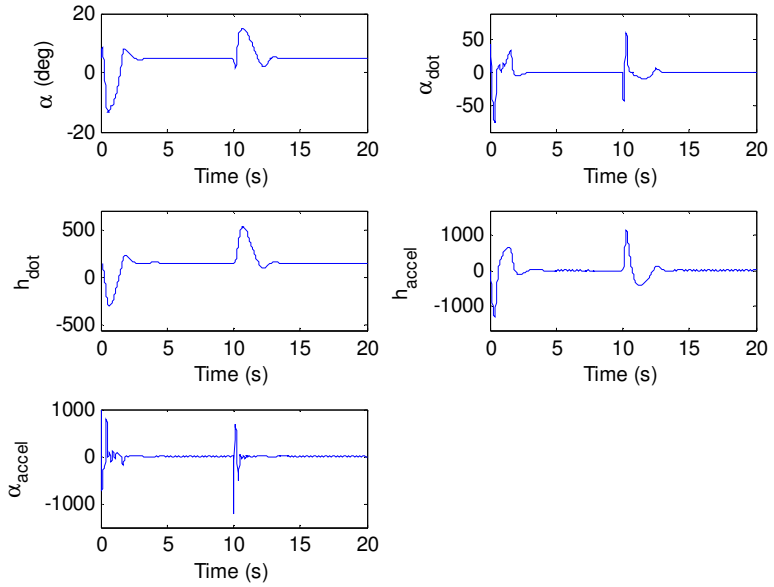

Figure 14. Inputs Used to Compute the Dynamic Response of the Control Surface Model

The response of the control surface is determined by the displacement of the point at the midchord on the tip of the control surface. This displacement is computed for both a square plate and a tapered, swept plate to compare the two. Figure 15 shows the computed displacements. Just before 19 seconds of heating the square plate begins to flutter, this is shown by the unbounded oscillations at the tip of the control surface. However, the tapered, swept plate does not show this response in the 20 second time. Also, the tapered, swept plate has a lower deflection throughout the entire simulation. Consequently, the reduced flexibility will cause the lifting characteristics of the control surface to match those of a rigid control surface more closely. This is beneficial because it was shown in Ref. [6] that there is a small decrease in the lift produced by a flexible control surface when compared to a rigid control surface.

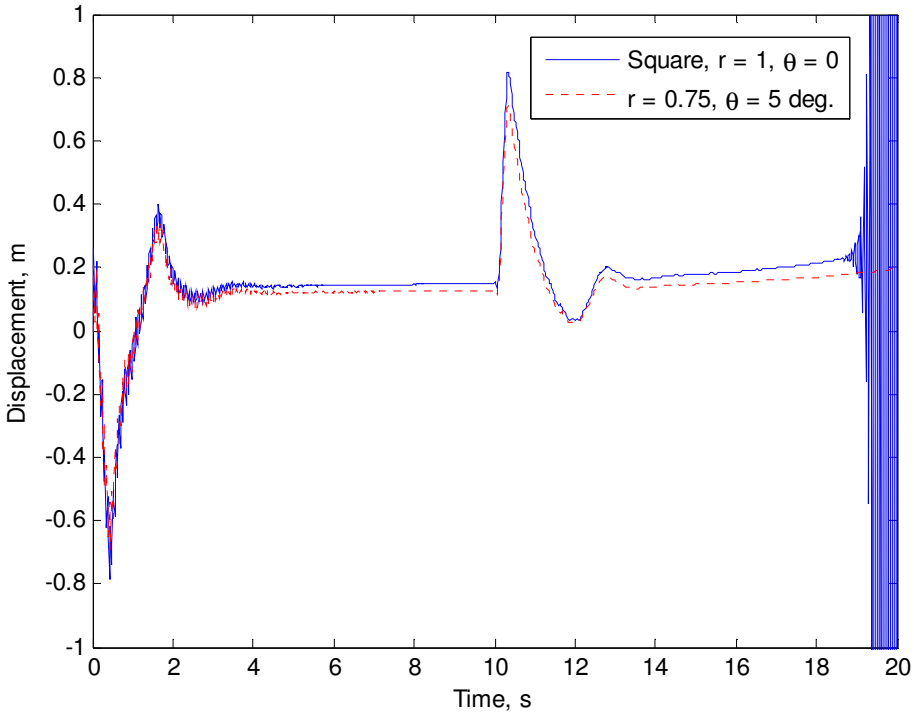

Figure 15. Tip Displacement Caused by Control Inputs

Conclusions

This research shows that the geometry of a control surface has a significant effect on the aerothermoelastic properties of a cantilever plate. Adding taper to the control surface increased the flutter Mach number. The flutter Mach number is increased uniformly over all temperatures for the temperature distribution prescribed in this research. This trend holds true over the range of r = 1 to 0.75. Additionally, as the sweep of the control surface is increased from 0 degrees to 5 degrees, the effect of heating becomes less. This means that as sweep is added, the flutter Mach number at high temperatures is higher, thus improving flutter characteristics.

These conclusions indicate that the effects of taper and sweep should be considered in order to develop an accurate model for a hypersonic control surface. However, the square plate underestimates the flutter Mach number, thus resulting in a conservative estimate of the aerothermoelastic response.

This research has resulted in an efficient model for a flexible, hypersonic control surface. This model could be used in conjunction with efficient models for the other systems on an air-breathing HSV, i.e. propulsion, airframe, and fuselage aerodynamics, to model the entire HSV in far less time than a high fidelity CFD and finite element model would take.

Matlab Functions

This section describes the Matlab functions implemented in this aerothermoelastic model of the hypersonic control surface. These functions generate the matrices described in the equations of motion.

The main Matlab functions of the model are:

- Pre_HSV_CS.m
- thermal_mtx.m
- ae_genforce.m
- HSV_CS_ae.m
- p_method.m

A. Pre_HSC_CS.m

This script serves as the preprocessor for the model. It only needs to be run once for each control surface configuration, i.e. a change in plate properties or geometry. The script computes the plate mass and stiffness matrices, $[\boldsymbol{M}]$ and $[\boldsymbol{K}]$, and also performs most of the spatial integrations required to generate the equations of motion.

The output from this script is stored in the **preproc_cs.mat** file. Since most of the integrations are carried out in this preprocessing step, the model is computationally efficient. The following inputs are required to run the preprocessing step:

- Plate Young's modulus
- Plate density
- Coefficient of Thermal Expansion
- Poisson's Ratio
- Length of the plate in the x-direction (spanwise direction)

- Length of the root chord in the y-direction (chordwise direction)
- Taper Ratio of the plate
- Sweep Angle of the plate
- Number of plate elements to use in the x and y direction (for numerical integration)
- Total number of Rayleigh-Ritz terms to include
- Total number of plate modes to retain (for plotting purposes and reducing the order of the aeroelastic equations of motion).
- Location of the pivot point of the all-moveable control surface.
- Aerodynamic surface slope (the current model assumes a symmetric double-wedge airfoil)

B. thermal_mtx.m

This function computes the incremental stiffness matrix due to thermal stresses, $[\boldsymbol{K^T}]$. Most of the input required by this file is provided in the **preproc_cs.mat** file. An additional required input is the temperature distribution.

C. ae_genforce.m

This function computes the generalized force vector, $\{\boldsymbol{Q}\}$, and the aerodynamic damping and stiffness matrices, $[\boldsymbol{C^A}]$ and $[\boldsymbol{K^A}]$. Most of the input for this file is provided by the **preproc_cs.mat** file. Additional required input is:

- Freestream Mach number
- Freestream dynamic pressure
- Freestream density
- Freestream speed of sound
- Freestream ratio of specific heats

- Control surface plunge rate due to fuselage motion.
- Control surface plunge acceleration due to fuselage motion.
- Control surface angle of attack.
- Control surface rate of change of angle of attack.
- Control surface acceleration of angle of attack.

D. HSV_CS_ae.m

This script solves the entire set of equations of motion described in Eqn. (12). The script uses a fourth order Runge-Kutta method to solve the set of ODEs. The input for this script is provided in the **preproc_cs.mat** file.

E. p_method.m

This script evaluates the homogeneous set of equations of motion to determine the flutter boundary at all temperatures. It requires the output file **preproc_cs.mat** as well as the thermal matrix, $[\boldsymbol{K^T}]$. Using these inputs this script computes the aerodynamic damping and stiffness matrices, $[\boldsymbol{C^A}]$ and $[\boldsymbol{K^A}]$, and solves for the flutter Mach number at each temperature increment.

References

[1] Walker, W. and Rodgers, F., "Falcon Hypersonic Technology Overview," *13th International Space Planes and Hypersonic Systems and Technologies Conference*, Capua Italy, 2005, AIAA 2005-3253.

[2] Bertin, J.J. and Cummings, R/M/, "Fifty Years of Hypersonics: Where We've Been and Where We're Going," *Progress in Aerospace Sciences*, Vol. 39, April 2003, pp. 511-536.

[3] Anderson, J.D., *Hypersonic and High Temperature Gas Dynamics*, McGraw-Hill, New York, 1989.

[4] Rasmussen, M., *Hypersonic Flow*, John Wiley & Sons, New York, 1994.

[5] Bertin, J.J., *Hypersonic Aerothermodynamics*, AIAA, 1994.

[6] McNamara, J.J., "Validation and Enhancements for a Control-Oriented Model of an Air-Breathing Hypersonic Vehicle," 2007 Summer Research Program Final Report, August 2007, AFRL/VACA, Wright-Patterson Air Force Base.

[7] Bailey, C.D., "Vibration of Thermally Stressed Plates with Various Boundary Conditions," *AIAA Journal*, Vol. 11, No. 1, 1973, pp. 14-19

[8] McNamara, J.J., *Aeroelastic and Aerothermoelastic Behavior of Two and Three Dimensional Surfaces in Hypersonic Flow*, Ph.D. thesis, University of Michigan, Ann Arbor, 2005.

[9] McNamara, J.J., and Friedmann, P.P., "Aeroelastic and Aerothermoelastic Analysis of Hypersonic Vehicles: Current Status and Future Trends," *48th AIAA/ASME/ASCE/AHS Structures, Structural Dynamics and Materials Conference*, Honolulu, HI, April 2007, AIAA 2007-2013.

[10] Chandrupatla, T.R. and Belegundu, A.D., *Introduction to Finite Elements in Engineering*, Prentice Hall, New Jersey, 1997.

[11] Lighthill, M.J., "Oscillating Airfoils at High Mach Numbers," Journal of the Aeronautical Sciences, Vol. 20, No. 6, June 1953.